SUPPLEMENTARY MATERIAL:

The one-dimensional camelback potential in the parallel dipole line trap: Stability conditions and finite size effect

Oki Gunawan and Yudistira Virgus
IBM T. J. Watson Research Center, Yorktown Heights, NY 10598
*Correspondence to: ogunawa@us.ibm.com.

Outline:

A. Materials

We use an experimental setup that we refer as "Reference PDL trap" consisting of specific magnets and graphite rods. The magnets are cylindrical neodymium iron boron (NdFeB) magnets with transverse magnetization (also called diametric magnet, KJ Magnetics, part number D4X0DIA-N52). The magnets' characteristics are: length L = (25.4±0.05) mm, radius a = (3.15±0.05) mm, and magnetization $M = (1.11\pm0.04)\times10^6$ A/m, thus they have aspect ratio of L/a = 8. The magnetization M was determined from fitting of near and far magnetic field data as shown and discussed in Fig. 2(c). The magnetic field was measured with Lakeshore 410 Gaussmeter (Sensor calibration# 787). For the graphite rods we used mechanical pencil leads (Pentel, "Hi Polymer") with hardness type “HB” with nominal diameter from 0.3 to 0.9 mm. The actual diameter (or radius) were measured using Mitutoyo (Model#293-344) micro caliper with 1 μm resolution. The mass were measured using micro balance (Metler AE100). The detail characteristics are shown in the table below:

Type	Nominal Diameter	Actual Radius (b)	Mass density (ρ)
	(mm)	(mm)	(kg/m^3)
HB	0.3	0.188±0.002	1583±45
HB	0.5	0.282±0.003	1693±32
HB	0.7	0.352±0.002	1682±22
HB	0.9	0.447±0.002	1680±14

Table S1. Characteristics of the graphite leads used in this experiment.

We refer to specific type of graphite rod as, for example, HB/0.5 which indicates a graphite rod type "HB" with nominal diameter 0.5 mm. We use magnetic susceptibility of $\chi = -(2.0\pm0.2)\times10^{-4}$ which was determined using the camelback oscillation period (Eq. 12) in our previous work [4].

B. Field of a Single Dipole Line System

B.1 Long dipole line system

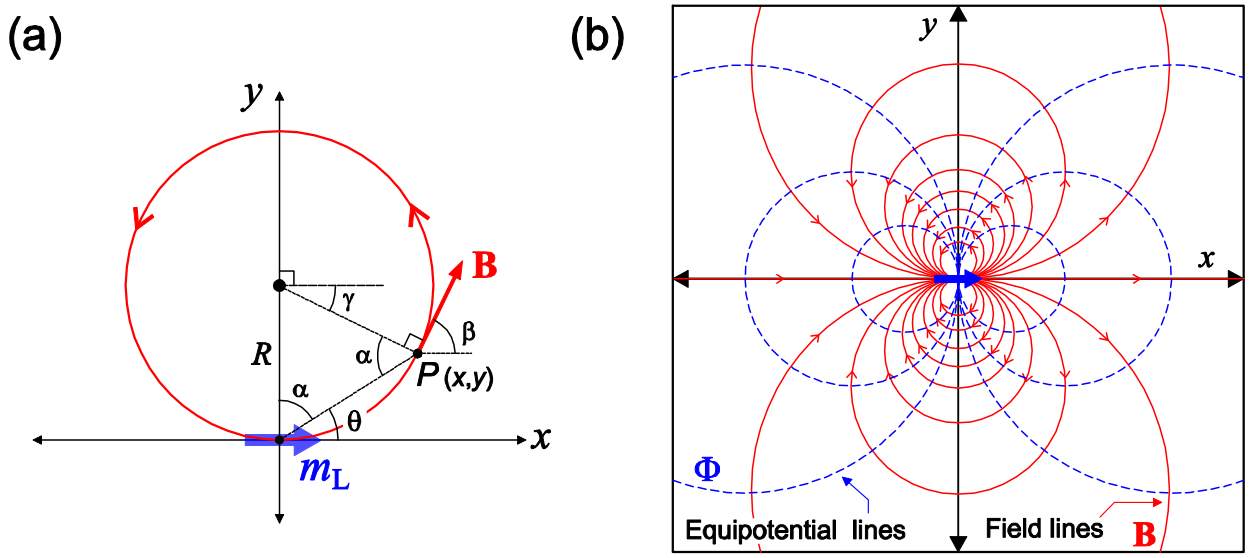

FIG. S1. (a) The field lines geometrical construction of a long dipole line system. (b) The field lines (**B** , red) and equipotential lines (**Φ**, dashed blue) of a long dipole line system.

In investigating the detailed field distribution around dipole line and diametric magnet system we discovered a curious and apparently overlooked mathematical property in this system: all the magnetic field lines form *perfect circles* as shown in Fig. 2(b) and Fig. S1 [32]. This fact can be

derived from the McDonald's formula for a long dipole line or long transversely-magnetized cylinder (Eq. 1) using the following approaches:

(1) Analytical method

Consider the field line at point P in Fig. S1. The slope along the field line obeys:

$$\frac{dy}{dx} = \frac{B_y}{B_x} = \frac{2\,x\,y}{x^2 - y^2} = \frac{2u}{1-u^2}, \qquad \text{where: } u = \frac{y}{x}. \tag{15}$$

We have: $\frac{du}{dx} = \frac{1}{x}\frac{dy}{dx} - u$, or : $\frac{dy}{dx} = u + x\frac{du}{dx}$, then:

$$u + x\frac{du}{dx} = \frac{2u}{1-u^2}\ , \text{or:} \qquad \frac{1-u^2}{u(1+u^2)}du = \frac{dx}{x} \tag{16}$$

Integrating both sides we obtain:

$$\ln\frac{u}{1+u^2} = \ln x + c_1\ , \text{or:} \qquad \frac{u}{(1+u^2)x} = c_2\ , \text{or:} \qquad x^2 + y^2 - y/c_2 = 0 \tag{17}$$

We can substitute the arbitrary constant c_2 as : $c_2 = 1/2R$, and rewrite the last equation as:

$$x^2 + (y-R)^2 = R^2 \tag{18}$$

Thus the field lines of a very long dipole line system is a family of circles with radius *R* and centered at (0, *R*).

(2) **Geometrical method**

Alternatively we also provide a shorter geometrical proof. Consider a closed loop of field line as shown in Fig. S1(a) above. We have $\gamma = 2\alpha - \pi/2$ and $\beta = \pi/2\text{-}\gamma$. The direction of the magnetic field at point P is equal to the gradient vector of the field lines whose slope is given as:

$$dy/dx = \tan\beta \tag{19}$$

From the McDonald's formula (Eq. 1) at point P we can calculate the slope:

$$\frac{dy}{dx} = \frac{B_y}{B_x} = \frac{2\,x\,y}{x^2 - y^2} = \frac{2\tan\theta}{1-\tan^2\theta} = \tan 2\theta \tag{20}$$

Thus: $\tan\beta = \tan 2\theta$, which is satisfied if: $\beta = 2\theta$ at every point along the closed loop which implies that the loop is a circle as shown in Fig. S1(a).

(3) **Conformal mapping with complex function method**

Besides our derivations above, K. T. McDonald has also pointed out [12] that we can obtain the field lines using conformal mapping function technique. For completeness we present again his derivation in Ref. 12 with additional comments below. Any complex function *f*(*z*) can be decomposed into its real and imaginary part function: $f(z) = \phi(z) + i\,\lambda(z)$ where *z* is the complex variable $z = x + i\,y$. The real and imaginary part of this function are harmonic functions that satisfy Laplace equation: $\nabla^2\phi = 0$ and $\nabla^2\lambda = 0$. The lines of constant ϕ represent equipotential lines and the lines of constant λ represent the field lines. These lines are orthogonal to each other as shown in Fig. S1(b). For the case of magnetic field we have $\mathbf{B} = -\mu_0 \nabla\Phi$. See also discussion in Ref. 33, Sec. 7.2. Unfortunately this technique is essentially an indirect method that requires some guesswork or a lucky coincidence in finding the correct complex function *f* (*z*) that corresponds to the physical situation at hand. It is also limited to two-dimensional problem and thus has limited applications.

For the case of a long dipole line system, fortunately there is a very simple conformal complex function associated with it, in the form of $f(z) = 1/z$ [12]. To be exact:

$$f(z) = \frac{Ma^2}{2z} = \frac{Ma^2}{2}\frac{x - i\,y}{x^2 + y^2} = \phi(x, y) + i\,\lambda(x, y) \ , \text{ where}$$

$$\phi = \frac{M\,a^2}{2}\frac{x}{x^2 + y^2}, \quad \text{and} \quad \lambda = -\frac{M\,a^2}{2}\frac{y}{x^2 + y^2} \tag{21}$$

This yields equipotential lines (lines of constant ϕ):

$$\left(x - R_\phi\right)^2 + y^2 = R_\phi^{\,2} \tag{22}$$

which are circles of radii $R_\phi = a^2 / M\,|\phi|$ centered at $(x, y) = (R_\phi, 0)$; and it also yields field lines (lines of constant λ):

$$x^2 + \left(y - R_\lambda\right)^2 = R_\lambda^{\,2} \tag{23}$$

which are circles of radii $R_\lambda = a^2 / M\,|\lambda|$ centered at $(x, y) = (0, R_\lambda)$. The plots of these function are given in Fig. S1(b).

The discussion of the $f(z) = z^{-1}$ complex potential function apparently first appeared in "The mathematical theory of electricity and magnetism" book (1908) by J. H. Jeans (who is also well known for the Rayleigh-Jeans law) [34]. This function appeared as a special case of a generalized $f(z) = z^n$ function where *n* = -1. Jeans noted that the equipotential and field lines are circles (Ref. 34, pg. 262,) however he did not comment on the physical context associated with this function. Later on, this function was also briefly mentioned in the "The Feynman Lecture on Physics, Vol. 2" (Ref. 33, Sec. 7.2, Eq. 7.15). Feynman indeed indicated that this function yields field distribution for the "*two-dimensional analog of an electric dipole, i.e., two parallel line charges with opposite polarities,*

very close together." It is curious that while Feynman noted that this function is associated with a "dipole line" system he did not show that the equipotential and field lines are *circles*; while showing many other potential line examples from various $f(z) = z^n$ conformal mapping functions. We think that the simplicity and symmetry appeal of the dipole line field and equipotential lines would serve as an excellent examples in discussing electromagnetic field and potential.

B.2 Finite length dipole line system

We consider a single transverse dipole line of finite length L as shown in Fig. 2(a). The dipole line points to x-direction with dipole moment per unit length: $m_L = m/L$ where m is the magnetic dipole moment. The magnetic field of a point dipole is given as: $\mathbf{B}(x, y) = \mu_0/4\pi \times [3(\mathbf{r}\cdot\mathbf{m})\hat{\mathbf{r}} - \mathbf{m}]/r^3$. We can expand this expression in Cartesian vector form:

$$\mathbf{B}(x, y, z) = \frac{\mu_0}{4\pi}\frac{m}{r^3}\begin{bmatrix} 3x^2/r^2 - 1 \\ 3xy/r^2 \\ 3xz/r^2 \end{bmatrix} \tag{24}$$

We want to calculate the field at point P. We consider the elemental dipole contribution at point S (0, 0, z_S) : $dm = m_L\, dz_S$. The position vector at point P is given as: $\mathbf{r} = \mathbf{P} - \mathbf{S} = [x, y, z - z_S]$, now we can calculate the total field at point P as:

$$\mathbf{B}_{DL}(x, y, z) = \frac{\mu_0}{4\pi}\frac{m_L}{r^3}\int_{-L/2}^{L/2}\begin{bmatrix} 3x^2/r^2 - 1 \\ 3xy/r^2 \\ 3x(z - z_S)/r^2 \end{bmatrix} dz_S \tag{25}$$

We obtain:

$$\mathbf{B}_{DL}(x, y, z) = \mu_0\frac{m_L}{4\pi}\sum_{n=1}^{2}\frac{(-1)^n}{(x^2 + y^2)^2(x^2 + y^2 + {w_n}^2)^{3/2}}\begin{bmatrix} w_n[(y^2 - x^2)(y^2 + {w_n}^2) - 2x^4] \\ -x\, y\, w_n(3x^2 + 3y^2 + 2{w_n}^2) \\ (x^2 + y^2)^2 x \end{bmatrix} \tag{26}$$

with $w_{1,2} = z \pm L/2$, which is the Eq. (2) in the main text.

For a very long dipole line system ($L >> a$), at the center plane $z = 0$, we have $w_{1,2} = (-1)^{n+1}\ (L/2)$. This equation now reduces to :

$$\mathbf{B}_{DL}(x, y) \approx \mu_0\frac{m_L}{4\pi}\sum_{n=1}^{2}\frac{(-1)^n}{(x^2 + y^2)^2(L/2)^3}\begin{bmatrix} (-1)^{n+1}(y^2 - x^2)(L/2)^3 \\ -(-1)^{n+1}2x\, y\,(L/2)^3 \\ (x^2 + y^2)^2 x \end{bmatrix} = \frac{\mu_0 m_L}{2\pi(x^2 + y^2)^2}\begin{bmatrix} x^2 - y^2 \\ 2x\, y \\ 0 \end{bmatrix} \tag{27}$$

which is the field formula of a very long transverse cylindrical magnet as was first derived by K. T. McDonald as shown in Eq. (1) [12].

For a finite length dipole line system, in near field ($r < r_T$) the field falls off as $B \propto 1/r^2$ which we refer as the dipole line limit and in far field ($r > r_T$) as $B \propto 1/r^3$ which we refer as the point dipole limit. The boundary between this near and far field regime can be estimated by considering the intersection of the asymptotical lines of this near and far field behavior. We consider the field distribution of a finite dipole line system pointing at x-direction as shown in Fig. 2(c). In the near field or dipole line limit the field can be approximated as a long dipole line system. We start from the long dipole line or McDonald's formula (Eq. 1) in polar coordinate:

$$\mathbf{B}_{DL}(r,\theta) = \frac{\mu_0 m_L}{2\pi r^2}[\cos\theta\hat{\mathbf{r}} + \sin\theta\hat{\boldsymbol{\theta}}] \tag{28}$$

Using $m_L = m/L$, the magnitude of the field only depends on the distance r where $r = \sqrt{x^2 + y^2}$:

$$B_{DL}(r) = \frac{\mu_0 a^2 m}{2\pi r^2 L} \tag{29}$$

In the far field or point dipole limit, the finite dipole line system will appear as a point dipole. Using a point dipole field formula we have:

$$\mathbf{B}_D(r,\theta) = \frac{\mu_0}{4\pi}\frac{m}{r^3}[2\cos\theta\hat{\mathbf{r}} + \sin\theta\hat{\boldsymbol{\theta}}] \tag{30}$$

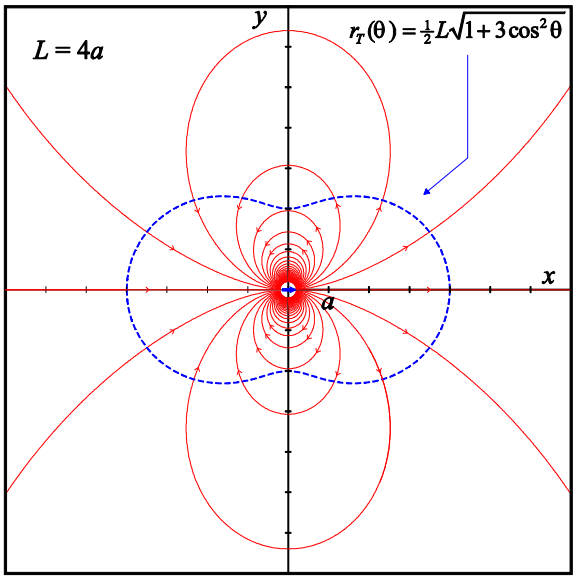

FIG. S2. The field lines of a dipole line system with *finite length* where $L = 4a$. The dashed curve marks the boundary that separates the dipole line regime (inside) and the point dipole regime (outside).

The magnitude of the field depends on the distance r and angular position θ:

$$B_D(r) = \frac{\mu_0}{4\pi}\frac{m}{r^3}\sqrt{3\cos^2\theta + 1} \tag{31}$$

The transition between the two regimes occurs at position $r_T(\theta)$ where $B_{DL}(r_T,\theta) = B_D(r_T,\theta)$:

$$r_T(\theta) = \tfrac{1}{2} L\sqrt{1+3\cos^2\theta} \tag{32}$$

This boundary is illustrated as a dashed curve in FIG. S2. Note that along the magnetization axis (i.e. $\theta = 0$ or *x*-axis, cf. FIG. S2) we have: $r_T = L$. This is an interesting rule of thumb which is easy to remember i.e. for a finite dipole line system with length *L*, the field along the dipole axis appears as a "*long dipole line*" for *r* << *L* and as a "*point dipole*" for *r* >> *L*. This characteristic is also very important for measurement of the magnet magnetization *M*. i.e. by measuring the field profile either at near field or far field in Eq. (29) and (31) above we can extract the value of *M* as illustrated in Fig. 2(c) in the main text.

B.3 Finite length diametric magnet

The magnetic field of a cylinder with transverse and uniform magnetization (or diametric magnet) with finite length *L* has been derived using magnetic scalar potential method in our previous work (Ref. 4, Supp. Mat. B) and is also shown in Eq. (3). We mentioned in the main text that this exterior field of a long (*L* >> *a*) diametric magnet is identical to that of a long dipole line system. This is analogous to the fact that *the field of a uniformly magnetized sphere is identical to that of a point dipole* [8, 35]. We provide the proof as follows.

We start with the general formula of a diametric magnet (Eq. 3). Now we consider a very long diametric magnet ($L \to \infty$) and set to calculate the field distribution only on the *x*-*y* plane (*z* = 0), thus we have $w_1 = L/2$ and $w_2 = -L/2$. Eq. (3) now becomes:

$$\mathbf{B}_{DM}(x,y,0) = \frac{\mu_0 Ma}{4\pi}\int_0^{2\pi}\sum_{n=1,2}\frac{(-1)^n\cos\phi}{w_n^{\,2}+s^2+w_n|w_n|(1+s^2/2w_n^{\,2})}\begin{bmatrix} x-a\cos\phi \\ y-a\sin\phi \\ w_n+|w_n| \end{bmatrix}d\phi \tag{33}$$

For *n* =1 and *z* = 0, the field vanishes: $\mathbf{B}_M(x,y) = [0,0,0]$ and thus we only need to consider *n* = 2 contribution :

$$\mathbf{B}_{DM}(x,y) = \frac{\mu_0 Ma}{2\pi}\int_0^{2\pi}\frac{\cos\phi}{(x-a\cos\phi)^2+(y-a\sin\phi)^2}\begin{bmatrix} x-a\cos\phi \\ y-a\sin\phi \\ 0 \end{bmatrix}d\phi \tag{34}$$

First, we calculate the integral for the *x*-component field. Note that we only consider the exterior field *i.e.* $(x^2+y^2) > a^2$:

$$I_X(x,y)=\int_0^{2\pi}\frac{(x-a\cos\phi)\cos\phi}{(x-a\cos\phi)^2+(y-a\sin\phi)^2}d\phi$$
$$=\frac{1}{4}\left(\frac{\phi[a^2(x^2-y^2)-(x^2+y^2)]}{a(x^2+y^2)^2}+\frac{a^2+(x-i\,y)^2}{a(x-i\,y)^2}\tan^{-1}\left[\frac{a\,y\cos\frac{1}{2}\phi-(a\,x+x^2+y^2)\sin\frac{1}{2}\phi}{(a\,x-x^2-y^2)\cos\frac{1}{2}\phi+a\,y\sin\frac{1}{2}\phi}\right]\right.$$
$$\left.-\frac{a^2+(x+i\,y)^2}{a(x+i\,y)^2}\tan^{-1}\left[\frac{(a\,x+x^2+y^2)\sin\frac{1}{2}\phi-a\,y\cos\frac{1}{2}\phi}{(a\,x-x^2-y^2)\cos\frac{1}{2}\phi+a\,y\sin\frac{1}{2}\phi}\right]\right)_0^{2\pi}=\frac{\pi a^2(x^2-y^2)}{(x^2+y^2)^2} \tag{35}$$

Next, we calculate the integral for the *y*-component :

$$I_Y(x,y)=\int_0^{2\pi}\frac{(y-a\sin\phi)\cos\phi}{(x-a\cos\phi)^2+(y-a\sin\phi)^2}d\phi$$
$$=\frac{1}{4a(x^2+y^2)^2}\left(2a^2xy\phi+4a^2x\,y\tan^{-1}\left[\frac{a\,y\cos\frac{1}{2}\phi-(a\,x+x^2+y^2)\sin\frac{1}{2}\phi}{(a\,x-x^2-y^2)\cos\frac{1}{2}\phi+a\,y\sin\frac{1}{2}\phi}\right]\right)_0^{2\pi} \tag{36}$$
$$=\frac{2\pi a\,x\,y}{(x^2+y^2)^2}$$

Given $M=m_L\pi a^2$, we finally arrive at the McDonald's formula for a long dipole line or long diametric magnet (Eq. 1) as expected:

$$\mathbf{B}_{DL}(x,y)=\frac{\mu_0 m_L}{2\pi(x^2+y^2)^2}[x^2-y^2,2\,x\,y,0] \tag{37}$$

C. Stability Condition in a PDL Trap: Jacobian Matrix Calculation

Stability requirement of a diamagnetic levitation system based on energy has been discussed by K. T. McDonald in Ref. 15, Appendix C. According to Lagrange, a system that can be described by potential energy $U(\mathbf{x}_e)$ at equilibrium point $\mathbf{x}_e$ where the force $F=-\nabla U=0$ is stable against small displacements if the energy U is a local minimum at $\mathbf{x}_e$. This condition can be evaluated by calculating the Jacobian matrix: $J_{ij}=\partial^2U(\mathbf{x}_e)/\partial x_i\partial x_j$. The system is stable at an equilibrium point against small displacements in any direction if the eigenvalues of the Jacobian matrix all have positive real parts.

We now evaluate the stability requirement of a PDL trap system in the small and short rod limit ($b \ll a$, $l \ll L$). In this limit, the total potential energy per unit rod volume (Eq. 9) simplifies to:

$$U_T'(x,y_0,z)=\rho g\,y_0-\chi B^2(x,y_0,z)/\mu_0(\chi+2) \tag{38}$$

We only consider the spatial degree of freedom (x, y, z) and no rotational ("yaw" or "pitch" rotation) degree of freedom. The latter implies that the long axis of the rod is always aligned with the z-axis (in reality for a very short rod $l < l_{\min}$, there is a "yaw" rotation that twists the rod as discussed in Section III.B, however we ignore this effect here).

To immediately address the stability condition we performed numerical computation (instead of analytical calculation) to calculate the Jacobian matrix. We use the following parameters for the PDL trap: $M = 10^6$ A/m, $L = 25.4$ mm and $a = 3.175$ mm, $\rho = 2000$ kg/m^3 and $\chi = -2\times10^{-4}$. We obtain the following Jacobian matrix:

$$\mathbf{J} = \begin{bmatrix} 1.4965 & 0 & 0 \\ 0 & 4.1434 & 0 \\ 0 & 0 & 0.00428 \end{bmatrix} \times 10^7 \text{ N/m}^4 \tag{39}$$

We obtain a diagonal matrix where the diagonal elements are the "spring constant" of the confinement potential along the corresponding axis i.e. $k'_i = J_{ii}$. In this case the criterion for stability reduces to $\partial^2 U(\mathbf{x}_e)/\partial^2 x_i > 0$, or $k'_i > 0$, for each coordinate x_i. This condition is indeed satisfied in our case - consistent with the experimental observation that the trap is stable against small displacement.

We also observe another notable characteristics from the Jacobian matrix, the ratio of these "spring constants" $k'_x : k'_y : k'_z = 349 : 967 : 1$ - which implies that the camelback potential along the longitudinal (z) axis is the weakest and the vertical (y-axis) confinement is the strongest. This fact is also apparent by comparing all the confinement potentials in x, y and z direction as shown in Fig. 3.

D. Camelback Spring Constant (k'_z) Calculation

Strictly speaking, for a short diamagnetic rod ($l << L$) placed at certain position z at the center of the trap ($x = 0$), the levitation height y_0 will vary along the z axis as the diamagnetic repulsion force: $F_y(\mathbf{r})$ varies along z. In fact the height profile follows the camelback profile as shown in FIG. S3. This occurs because $F_y(\mathbf{r}) \propto -B(\mathbf{r})\partial B(\mathbf{r})/\partial y$. We show that in calculating the spring constant k'_z at the center of the trap ($z = 0$), we can assume that y_0 is independent of z.

We consider the total energy as a function of y_0 which depends on z *i.e.* $y_0(z)$:

$$U(x, y_0, z) = U_M(x, y_0(z), z) + \rho g y_0(z) \tag{40}$$

The first derivative ($x = 0$) :

$$\frac{\partial U(y_0(z), z)}{\partial z} = \frac{\partial U(y_0(z), z)}{\partial y_0}\frac{\partial y_0}{\partial z} + \frac{\partial U(y_0(z), z)}{\partial z} \tag{41}$$

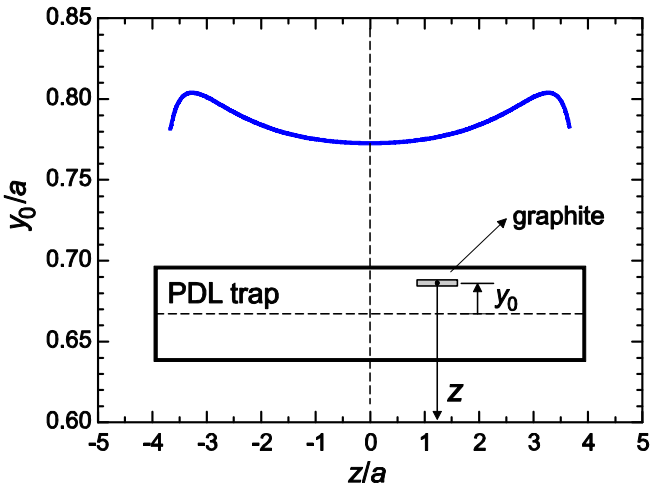

FIG. S3. The variation of levitation height as a function of the position z calculated using PDM field model (Eq. 3 and 4) for short and small diamagnetic rod in the Reference PDL trap.

The second derivative:

$$\frac{\partial^2 U(y_0(z),z)}{\partial z^2}=\frac{\partial^2 U(y_0(z),z)}{\partial y_0 \partial z}\frac{\partial y_0}{\partial z}+\frac{\partial U(y_0(z),z)}{\partial y_0}\frac{\partial^2 y_0}{\partial z^2}+\frac{\partial^2 U(y_0(z),z)}{\partial z^2} \tag{42}$$

Since the rod is always at vertical equilibrium: $\partial U(y_0(z),z)/\partial y_0 = 0$, thus :

$$\frac{\partial^2 U(y_0(z),z)}{\partial z^2}=\frac{\partial^2 U(y_0(z),z)}{\partial y_0 \partial z}\frac{\partial y_0}{\partial z}+\frac{\partial^2 U(y_0(z),z)}{\partial z^2} \tag{43}$$

Then at the center of the trap ($z = 0$): $\partial y_0/\partial z = 0$, thus the spring constant :

$$k_z=\frac{\partial^2 U(y_0(z),z)}{\partial z^2}=\left.\frac{\partial^2 U(y_0,z)}{\partial z^2}\right|_{z=0} \tag{44}$$

which is the same as our original derivation where we assume a constant levitation height y_0.

E. The Critical Length of the Camelback Potential

The camelback potential only occurs when the length of the system is beyond certain critical length L_C. We will derive the condition for L_C using both the PDL and PDM model. To determine L_C it is sufficient to consider the second derivative of the magnetic field profile $B_x(z)$. The existence of the camelback humps on both edges imply that the curvature of $B(z)$ is positive (i.e. $\partial^2 B/dz^2 > 0$). We can obtain the critical length L_C when the curvature of the magnetic profile is zero i.e. $\partial^2 B/dz^2 = 0$ or equivalently $\partial^2 B^2/dz^2 = 0$. This is because $\partial^2 B^2/\partial z^2 = 2\left[(\partial B/\partial z)^2 + B(\partial^2 B/\partial z^2)\right]$, and at the center of the trap we have: $\partial B/dz = 0$, thus:

$$\frac{\partial^2 B^2}{\partial z^2} = 2B\left(\frac{\partial^2 B}{\partial z^2}\right) \tag{45}$$

This relationship allows us to use the expression for the camelback spring constant k_z that we have obtained, $k'_z = -\chi/\mu_0(2+\chi)\times\partial^2 B^2(0, y_0, 0)/\partial z^2$:

$$k'_z(y_0, L) = -\frac{\mu_0 M^2}{L^2}\frac{\chi}{2+\chi}\frac{96\,\bar{L}^4(\bar{L}^2 + 4\bar{y}_0^{\,2} - 16)[(\bar{L}^2 + 4\bar{y}_0^{\,2})(1-\bar{y}_0^{\,2}) + 8]}{(1+\bar{y}_0^{\,2})^2(4+\bar{L}^2+4\bar{y}_0^{\,2})^5} \tag{46}$$

At the critical length L_C we have $k'_z = 0$, and considering that the levitation height: $|\bar{y}_0| < 1$, the roots only come from the term: $\bar{L}^2 + 4\bar{y}_0^{\,2} - 16 = 0$. Thus we obtain the critical length L_C:

$$L_C = 2\sqrt{4a^2 - y_0^{\,2}} \tag{47}$$

For the experimental context using PDM system we have to perform numerical calculation of k'_z (y_0, L) with magnetic field calculated using the PDM model (Eq. 3 and 4). We solve for L_C where $k'_z(y_0, L) = 0$ at different y_0. The result is plotted as the red curve in Fig. 4(c).

F. The Linear Charge Model of a PDL System

We now investigate the origin of the camelback humps using fictious charge model of the PDL system as shown in Fig. 5(a). There are two dipole lines on the x-z plane. To obtain some insights to the origin of the camelback effect, we partition the dipole lines into separate lines of charges. First we will calculate the magnetic field at point P(0, y, z) due to ***a pair*** distribution of linear charge $\pm\lambda = q/L$ labeled Q and Q' located at $x = \pm x_Q$ from $z = -L/2$ to $+L/2$ as shown in Fig. 5(a).

The elemental magnetic field at point P is given as:

$$d\mathbf{B}_Q = \frac{\mu_0 dq}{4\pi r^3}[x_Q\,\hat{\mathbf{x}} + y\hat{\mathbf{y}} + (z - z_Q)\hat{\mathbf{z}}] \quad \text{and} \quad d\mathbf{B}_{Q'} = -\frac{\mu_0 dq}{4\pi r^3}[-x_Q\hat{\mathbf{x}} + y\hat{\mathbf{y}} + (z - z_Q)\hat{\mathbf{z}}] \tag{48}$$

where $\mathbf{r}^2 = x_Q^{\,2} + y^2 + (z - z_Q)^2$.

The elemental magnetic field due to this linear charge is:

$$d\mathbf{B}_{DL}(0, y, z) = d\mathbf{B}_Q + d\mathbf{B}_{Q'} = \frac{\mu_0 dq}{4\pi}\frac{x_Q}{r^3}\hat{\mathbf{x}} \tag{49}$$

where the magnetic field only has x-component. Thus the total magnetic field at point P due to a single dipole line is given as :

$$\mathbf{B}_{DL}(0,y,z)=\frac{\mu_0\lambda x_Q}{4\pi}\int_{-L/2}^{L/2}\frac{dz_P}{r^3}\hat{\mathbf{x}}=\frac{\mu_0\lambda x_Q\hat{\mathbf{x}}}{(x_Q{}^2+y^2)}\frac{z_Q-z}{\sqrt{x_Q{}^2+y^2+(z-z_Q)^2}}\Bigg|_{z_Q=-L/2}^{z_Q=L/2} \tag{50}$$

$$\mathbf{B}_{DL}(0,y,z)=\frac{\mu_0\lambda x_Q\hat{\mathbf{x}}}{(x_Q{}^2+y^2)}\left(\frac{L/2-z}{\sqrt{x_Q{}^2+y^2+(z-L/2)^2}}+\frac{L/2+z}{\sqrt{x_Q{}^2+y^2+(z+L/2)^2}}\right) \tag{51}$$

Now we consider the complete PDL system as shown in Fig. 5(a), here we have the inner (red) and outer (blue) dipole lines placed at $x_Q=a-d/2$ and $x_Q=a+d/2$ respectively. We can plot the resulting magnetic field as shown in Fig. 5(b). The inner line contributes to a large and positive field profile that looks like a peak, however the outer line contributes to a smaller and negative field with more gentle profile because they are further apart. The mismatch of these field profiles at the edges produce the *camelback humps*.

Now we can calculate the total magnetic field of the overall PDL system:

$$\mathbf{B}_{PDL}(0,y,z)=\mathbf{B}_{DL,in}(0,y,z)+\mathbf{B}_{DL,out}(0,y,z) \tag{52}$$

The upper and lower charge lines consist of linear distribution of point dipoles $p=Qd$ where $d<<a$. They form a dipole line with $m_L=\lambda d$, and we can calculate the total PDL field:

$$\mathbf{B}_{PDL}(0,y,z)=\mathbf{B}_{DL,in}(0,y,z)+\mathbf{B}_{DL,out}(0,y,z) \tag{53}$$

$$\mathbf{B}_{DL,in}(0,y,z)=\mathbf{B}_{DL}(0,y,z)\big|_{x_Q=a}+\partial\mathbf{B}_{DL}/\partial x_Q(0,y,z)\times\tfrac{1}{2}d \tag{54}$$

$$\mathbf{B}_{DL,out}(0,y,z)=-\mathbf{B}_{DL}(0,y,z)\big|_{x_Q=a}-\partial\mathbf{B}_{DL}/\partial x_Q(0,y,z)\times(-\tfrac{1}{2}d) \tag{55}$$

The first term cancels off:

$$\mathbf{B}_{PDL}(0,y,z)=\partial\mathbf{B}_{DL}/\partial x_Q(0,y,z)\big|_{x_Q=a}\times d \tag{56}$$

$$\mathbf{B}_{PDL}(0,y,z)=\frac{\mu_0\lambda\, a\, d}{(a^2+y^2)^2}\frac{[2a^4+(a^2-y^2)(y^2+(z-z_Q)^2)](z-z_Q)}{(a^2+y^2+(z-z_Q)^2)^{3/2}}\Bigg|_{z_Q=-L/2}^{z_Q=L/2}\hat{\mathbf{x}} \tag{57}$$

Normalizing the coordinates with respect to a we have:

$$\mathbf{B}_{PDL}(0,y,z)=\frac{\mu_0 m_L a}{(1+\bar{y}^2)^2}\frac{(z-z_Q)[2+(1-\bar{y}^2)(\bar{y}^2+(z-z_Q)^2)]}{(1+\bar{y}^2+(z-z_Q)^2)^{3/2}}\Bigg|_{z_Q=-L/2}^{z_Q=L/2}\hat{\mathbf{x}} \tag{58}$$

which leads to the same PDL field equation given in Eq. (6):

$$\mathbf{B}_{PDL}(y,z) = \frac{\mu_0 m_L}{2\pi a^2 (1+\bar{y}^2)^2} \sum_{n=1}^{2} \frac{(-1)^n \bar{w}_n [(\bar{y}^2 - 1)(\bar{y}^2 + \bar{w}_n{}^2) - 2]}{(1+\bar{y}^2 + \bar{w}_n{}^2)^{3/2}} \hat{\mathbf{x}} \tag{59}$$

where the $\bar{y} = y/a$ and $\bar{w}_n = (z \pm L/2)/a$.

G. Stokes Drag and the Damped Oscillation of the Rod

In this section we present a simple theoretical model to calculate the viscous Stokes drag and the damping time constant of a cylindrical rod that oscillates along the camelback potential. We will model the cylinder as a prolate ellipsoid that moves along its major axis through an unbounded viscous fluid (a gas or air) with viscosity μ_F. The ellipsoid has semi-minor axis b equals to the radius of the cylinder and the semi-major axis c equals to half of the cylinder length l as shown in FIG. S4(a). Furthermore we will use a long prolate ellipsoid approximation where $l >> b$. This provides a simple and intuitive model that displays clear dependence of the drag with respect to its geometrical factors such as length and radius of the rod. We will also compare this model with a more realistic empirical Stokes drag model of cylindrical object that has been developed by Ui and coworkers [21].

The viscous drag of the prolate ellipsoid moving along its major axis in an unbounded fluid is given in Ref. 23, Section 4.30, as :

$$F_D = 6\pi\mu_F b K' v \tag{60}$$

where μ_F is the viscosity of the fluid, b is the semi-minor axis of the ellipsoid and v is the velocity of the object. K' is a "shape factor" of the Stokes drag that can be interpreted as the ratio of the drag force of the object with that of a sphere with equal cross section i.e. a circle with radius b. For a spherical object, we have $K' = 1$ as indicated by a solid circle in Fig. S4(b), which leads to the familiar Stokes drag equation of a sphere.

The factor K' for a prolate ellipsoid is given in Ref. 23, Section 4.30:

$$K' = \frac{4}{3\sqrt{\alpha^2 - 1}\left[(\alpha^2 + 1)\coth^{-1}\alpha - \alpha\right]} \tag{61}$$

where $\alpha = 1/\sqrt{1-(b/c)^2}$. In this work, we approximate the cylindrical rod of length l with a prolate ellipsoid with major and minor axis c and b respectively, thus we have $l = 2c$.

For a long prolate ellipsoid where $c >> b$, Eq. (61) can be simplified to:

$$K' = \frac{2c}{3b\left[\ln(c/b) + \ln 2 - 1/2\right]} = \frac{l}{3b\ln(0.607\, l/b)} \tag{62}$$

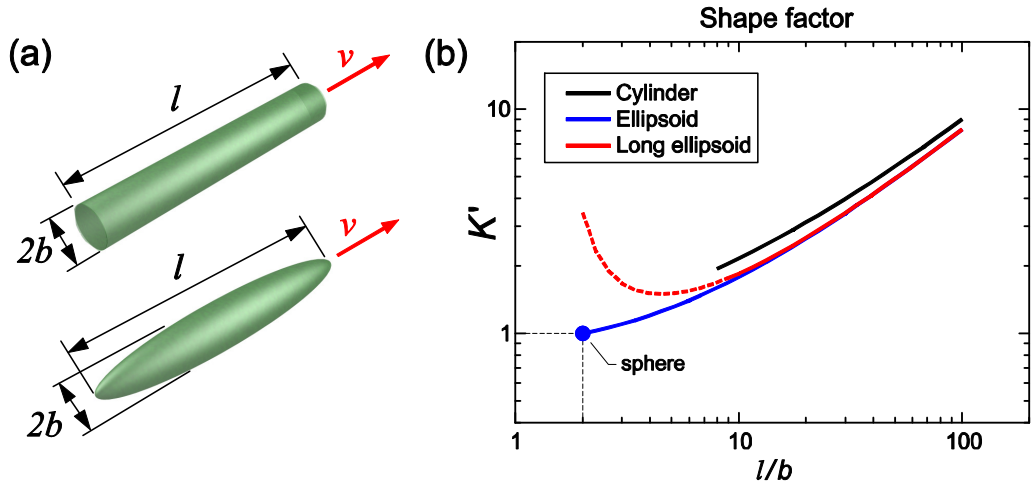

FIG. S4.(a) Cylindrical and prolate ellipsoid rod model for Stokes drag calculation. (b) The shape factor of the Stokes drag K' as a function of object aspect ratio: l/b for three geometry models: cylinder (Eq. 63), ellipsoid (Eq. 61) and a very long ellipsoid (Eq. 62). The solid circle at l/b =2 indicates the case for a sphere where K' = 1.

A more accurate description of the Stokes drag in a cylindrical body moving along its long axis has been studied by Ui and coworkers [21]. Unfortunately, unlike the case for sphere or ellipsoid, there is no exact analytical solution for the Stokes drag of a cylinder. Nevertheless they have developed an empirical model for a long cylinder [21]:

$$K_C' = \frac{l}{3b}(0.0244 + 0.5504\varepsilon + 3.328\varepsilon^2 - 2.971\varepsilon^3) \tag{63}$$

where $\varepsilon = 1/\ln(l/b)$. This formula is applicable for $8 < l/b < 148$ (or equivalently $0.48 < \varepsilon < 0.2$) [21]. It agrees well with the experimental data. Therefore in the main text we use the simpler long prolate ellipsoid model (Eq. 62) to illustrate the essential physics of the Stokes drag particularly the dependence on the size of the rod (radius and length).

We plot the coefficient K' for three rod geometries in FIG. S4: (1) A cylinder (2) A prolate ellipsoid (3) A long prolate ellipsoid. We make several observations: the ellipsoid model yields K' about 16% less than the cylindrical model - this is reasonable as an ellipsoid has smoother surface that has lower drag. At l/b = 2 the ellipsoid becomes a sphere and yield K' = 1 (indicated by solid circles). We note that the long prolate ellipsoid model (Eq. 37) agrees very well with the general ellipsoid drag model (Eq. 36) for $l/b > 10$.

Using the long prolate ellipsoid model (Eq. 62) we can calculate the damping time constant τ of the oscillating rod in a PDL trap. We model the motion as a damped harmonic oscillator in the presence of a viscous drag force: $F = -k_D v$. In such system, the damping time constant is given as: $\tau = 2m/k_D$ where m is the mass of the object, and ellipsoid volume $V = \frac{2}{3}\pi b^2 l$, which yields:

$$\tau = 2\rho b^2 \ln(0.607 l/b)/3\mu_F \tag{64}$$

where ρ is the mass density of the object. This relationship is used to provide qualitative explanation of the experimental data as shown in Fig. 9.

In this calculation we assume a laminar flow (Stokes drag) regime, thus it is worthwhile to check the Reynolds number (Re) in this system which is given as: $\mathrm{Re} = \rho_F \, l \, v / \mu_F$ where ρ_F is the fluid (air) mass density. For our experiment plotted in Fig. 8(a) we have $\rho_F = 1.28$ kg/m^3, rod length $l = 4.5$ mm, radius b=0.45 mm, maximum velocity $v \sim 20$ mm/s and $\mu_F = 18.19$ μPa.s [22]. We obtain Re = 6.3, which is much smaller than 4000 where turbulent flow approximately starts to occur (Ref. 36, pg. 207) thus we confirm that our system is in the low Reynolds number regime.

Additional Acknowledgement:

Part of this work for gas characterization application was prepared as an account of work sponsored by an agency of the United States government (ARPA-E, Dept. of Energy Award Number DE-AR0000540). Neither the United States government nor any agency thereof, nor any of their employees, makes any warranty, expressed or implied, or assumes any legal liability or responsibility for the accuracy, completeness, or usefulness of any information, apparatus, product, or process disclosed, or represented that its use would not infringe privately owned rights. Reference herein to any specific commercial product, process, or service by trade name, trademark, manufacturer, or otherwise does not necessarily constitute or imply its endorsement, recommendation, or favoring by the United States government or any agency thereof. The views and opinions of authors expressed herein do not necessarily state or reflect those of the United States government or any agency thereof.

Additional References:

[32] O. Gunawan, "The parallel dipole line system, its camelback effect and fascinating applications: A novel electromagnetic trap and high sensitivity Hall system", Princeton PRISM/PCCM Spring Seminar Series, April 20, 2016.

[33] R. P. Feynman, R. B. Leighton, and M. Sands, *The Feynman lectures on physics, Vol. 2: Mainly electromagnetism and matter* (Addison-Wesley, 1979).

[34] J. H. Jeans, *The mathematical theory of electricity and magnetism* (University Press, Cambridge, 1908).

[35] D. J. Griffiths, *Introduction to electrodynamics*, 3rd ed. (Prentice Hall, Upper Saddle River, NJ, 1999).

[36] J. P. Holman, *Heat Transfer*, 9th ed. (McGraw-Hill, 2002).